MOX-Report No. 76/2020

Functional Regression Control Chart

Centofanti, F.; Lepore, A.; Menafoglio, A.; Palumbo, B.;

Vantini, S.

MOX, Dipartimento di Matematica
Politecnico di Milano, Via Bonardi 9 - 20133 Milano (Italy)

mox-dmat@polimi.it http://mox.polimi.it

Functional Regression Control Chart

Fabio Centofanti[1], Antonio Lepore[1], Alessandra Menafoglio[2], Biagio Palumbo*[1], and Simone Vantini[2]

[1]*Department of Industrial Engineering, University of Naples Federico II, Piazzale Tecchio 80, 80125, Naples, Italy*

[2]*MOX - Modelling and Scientific Computing, Department of Mathematics, Politecnico di Milano, Piazza Leonardo da Vinci 32, 20133, Milan, Italy*

This is an Author's original manuscript of an article published by Taylor & Francis in Technometrics on April 4, 2020, available at `https://www.tandfonline.com/10.1080/00401706.2020.1753581.`

Abstract

The modern development of data acquisition technologies in many industrial processes is facilitating the collection of quality characteristics that are apt to be modelled as functions, which are usually referred to as *profiles*. At the same time, measurements of concurrent variables, which are related to the quality characteristic profiles, are often available in a functional form as well, and usually referred to as *covariates*. In order to adjust the monitoring of the quality characteristic profiles by the effect of this additional information, a new functional control chart is elaborated on the residuals obtained from a function-on-function linear regression of the quality characteristic profile on the functional covariates. Furthermore, by means of a Monte Carlo simulation study, the performance of the proposed control chart are compared with those of other charts proposed in the literature. Eventually, a real-case study in the shipping industry is presented with the purpose of monitoring ship fuel consumption and thus, CO_2 emissions from a Ro-Pax ship, with particular regard to detecting CO_2 emission reduction after a specific energy efficiency initiative.

Keywords: Functional Data Analysis, Multivariate Functional Linear Regression, Profile Monitoring, Statistical Process Control

*Corresponding author. e-mail: `biagio.palumbo@unina.it`

1 Introduction

In many industrial contexts, the development in data acquisition systems allow massive amounts of data to be recorded at high-rate and modelled as functions defined on multidimensional domains, i.e., *functional data* (Ramsay, 2005; Ferraty and Vieu, 2006; Hsing and Eubank, 2015). In this scenario, new *statistical process control* (SPC) methods must be developed to monitor and control the stability over time of the quality characteristic, when functional data are available. In the classical SPC literature, functional data are more often referred to as *profiles* (Woodall et al., 2004). An overview of the main achievements in profile monitoring can be found in Noorossana et al. (2012). Other relevant contributions include the works of Jin and Shi (1999); Colosimo and Pacella (2010); Grasso et al. (2016, 2017); Menafoglio et al. (2018). As in the classical SPC (i.e., where data are scalars) profile monitoring control charts have the task of continuously monitoring the quality characteristic and of triggering a signal when assignable sources of variations (i.e. *special causes*) act on it. When this happens, the process is said to be out-of-control (OC). On the contrary, the process is said to be in-control (IC) when only normal sources of variation (i.e., *common causes*) apply.

In practice, there are situations where the quality characteristic is influenced by one or more covariates. In this scenario, if one of these covariates manifests itself with an extreme realization, the quality characteristic may wrongly be judged to be OC. Otherwise, there may be situations where the covariates are not extreme and the quality characteristic may wrongly appear IC. As well as, the quality characteristic may wrongly appear IC, because the variance explained by the covariates is overlooked. In the multivariate SPC literature these issues have been addressed by means of the *regression control chart* (RCC) (Mandel, 1969). The basic idea behind this chart is to consider the quality characteristic after being adjusted for the effects of the covariates, that is monitoring the residuals of the regression of the quality characteristic on the covariates. Hawkins (1991) applied this idea to the multivariate setting by considering the regression of a variable on covariates that are assumed to be IC, and developed *Shewhart* and *cumulative sum* (CUSUM) control charts (Montgomery, 2007) based on the regression residuals. Hawkins (1993) applied the regression adjustment to particular kind of processes, said cascade processes in order to

take advantage of the correlation between measures. Another application of the idea of regression adjustment appeared in Wade and Woodall (1993) where the so called cause-selecting control chart has been used for monitoring and control multistage processes. Other studies on the RCC include those of Shu et al. (2004), which studied the effects of the parameter estimation on the run length performance of the control chart, and those of Zhou and Goh (2016), where the influence of the regression model choice on the control chart performance was analysed.

In the literature of the RCC, the model used to describe the relation between the quality characteristic (hereinafter referred to also as *response variable*) and the covariates (hereinafter referred to also as *predictor variables*) is the linear regression model. In the functional context, functional linear regression models with one scalar response and one functional covariate have been deeply analysed in Cardot et al. (2003) and Hall et al. (2007); whereas, the extension to functional response was study by Ramsay (2005) and Yao et al. (2005a). Functional linear models with functional response and multiple functional covariates have been far less studied. Matsui et al. (2009) developed estimation and evaluation methods based on regularized functional regression, whereas Fan et al. (2014) introduced the *functional response additive model estimation* (FRAME) and applied it to a case study in the online virtual stock markets. Chiou et al. (2016) proposed a functional liner model where both the response and the predictor variables are multivariate functional data, which relies on the *multivariate functional principal component* (MFPC) (or Karhunen–Loève) decomposition (Chiou et al., 2014; Happ and Greven, 2018).

In this paper, we propose a new framework for monitoring a functional quality characteristic when functional covariates are available. This framework is henceforth referred to as *functional regression control chart* (FRCC) and can be regarded as an extension of the RCC to the functional context. In particular, we consider the case when the model which links the functional response and functional covariates is linear and, we monitor residuals by using the profile monitoring approach introduced by Woodall et al. (2004) and then used in Noorossana et al. (2012); Grasso et al. (2016); Pini et al. (2018), which is based on the simultaneous application of the *Hotelling*'s T^2 and the squared prediction error (SPE) control charts.

A Monte Carlo simulation study is performed to quantify the FRCC *average run length* (*ARL*) (Montgomery, 2007), in identifying mean shifts in the functional response in presence or absence of drifts in the covariate means. This is done by comparing the proposed FRCC with other two control charts widely used in both the industrial context and the literature. In addition, a real-case study in the shipping industry is presented to illustrate the practical applicability of the proposed control chart. In particular, the FRCC is shown to adequately identify reductions of cumulative fuel consumption, and thus CO_2 emissions (which are stoichiometrically related to it) after an energy efficiency initiative (EEI) was performed off-line on the considered Ro-Pax ship. In addition, a functional bootstrap procedure is developed and applied to evaluate uncertainty of the obtained results.

The paper is structured as follows. Section 2 introduces the proposed FRCC. In Section 3 the performance of the FRCC is compared to that of other two popular control charts used for the same purpose. The real-case study is presented in Section 4. Section 5 concludes the paper. Supplementary Materials for the article are available online. All computations and plots have been obtained using the programming language R (R Core Team, 2018).

2 The Functional Regression Control Chart Framework

The proposed FRCC can be regarded as a general framework for profile monitoring that can be divided into three main steps. Firstly, (i) define a functional regression model to be fitted

$$Y = g(\mathbf{X}) + \varepsilon, \tag{1}$$

where Y is the functional response variable and ε is a functional error term, both defined on the compact domain $\mathcal{T}$, g is a generic function of a vector $\mathbf{X}$ of random functional covariates $X_1, \ldots, X_p$, defined on the compact domain $\mathcal{S}$.

Secondly, (ii) define the estimation method of the chosen model, and, thirdly (iii) define the monitoring strategy of the functional residual defined as

$$e = Y - \hat{Y}, \tag{2}$$

where $\hat{Y}$ is the fitted value of Y.

In what follows, after some preliminaries, we describe the FRCC when the following choices are made: (i) the *multivariate functional linear regression* (MFLR) model (Section 2.1) is set for the first step, (ii) an estimation method based on the Karhunen-Loève's decomposition (Section 2.2) is chosen for the second, and (iii) the *Hotelling*'s T^2 and the *squared prediction error* (SPE) control charts (Section 2.3) are built in the third step.

Preliminaries

Assume that $X_1, \ldots, X_p$ and Y have smooth realizations in $L^2(\mathcal{S})$ and $L^2(\mathcal{T})$, i.e., the Hilbert spaces of square integrable functions defined on the compact sets $\mathcal{S}$ and $\mathcal{T}$, respectively. Moreover, let us denote with $\mathbb{H}^X = (L^2(\mathcal{S}))^p$ the Hilbert space whose elements are vectors of functions in $L^2(\mathcal{S})$. Then, $\mathbf{X} = (X_1, \ldots, X_p)^T$ is random vector of functions whose realizations are in $\mathbb{H}^X$. Accordingly, for a compact set $\mathcal{Z}$, the inner product of two functions f and g in $L^2(\mathcal{Z})$ is $\langle f, g \rangle = \int_{\mathcal{Z}} f(z)\, g(z)\, dz$, with dz the Lebesgue measure on $\mathcal{Z}$, and the norm is $\|\cdot\| = \sqrt{\langle \cdot, \cdot \rangle}$. The inner product of two function vectors $\mathbf{f} = (f_1, \ldots, f_p)^T$ and $\mathbf{g} = (g_1, \ldots, g_p)^T$ in $\mathbb{H}^X$ is $\langle \mathbf{f}, \mathbf{g} \rangle_{\mathbb{H}^X} = \sum_{i=1}^{p} \langle f_i, g_i \rangle$ and the norm is $\|\cdot\|_{\mathbb{H}^X} = \sqrt{\langle \cdot, \cdot \rangle_{\mathbb{H}^X}}$. Further, assume that $\mathbf{X}$ has mean function $\boldsymbol{\mu}^X = \left(\mu_1^X, \ldots, \mu_p^X\right)^T$, with $\mu_i^X = \mathrm{E}(X_i)$ and covariance function $\mathbf{C}^X = \{C_{i,j}^X\}_{1 \le i,j \le p}$, with $C_{i,j}^X(s_1, s_2) = \mathrm{Cov}(X_i(s_1), X_j(s_2))$, for $s_1, s_2 \in \mathcal{S}$. Analogously, let $\mu^Y = \mathrm{E}(Y)$ and $C^Y(t_1, t_2) = \mathrm{Cov}(Y(t_1), Y(t_2))$, for $t_1, t_2 \in \mathcal{T}$, be the mean and the covariance function of the response variable $Y(t)$, respectively.

The transformation approach of Chiou et al. (2014) is here used, as covariates can exhibit different amount of variation. In what follows, all the operations between functions have to be considered pointwise. Let $\mathbf{X}^{std} = \left(X_1^{std}, \ldots, X_p^{std}\right)^T = \left(\mathbf{V}^X\right)^{-1} \left(\mathbf{X} - \boldsymbol{\mu}^X\right)$, be the vector of the standardized covariates, with the matrix $\mathbf{V}^X = \mathrm{diag}\left(\left(v_1^X\right)^{1/2}, \ldots, \left(v_p^X\right)^{1/2}\right)$ where $v_i^X(s) = C_{i,i}^X(s, s)$, for $s \in \mathcal{S}$. The response variable Y is also standardized as $Y^{std} = \left(v^Y\right)^{-1/2} \left(Y - \mu^Y\right)$, with $v^Y(t) = C^Y(t, t)$, for $t \in \mathcal{T}$. Let $\mathbf{C}_{std}^X$ and C_{std}^Y be the covariance functions of the standardized covariate and response variables, respectively. Let us consider for $\mathbf{C}_{std}^X$ the expansion $\mathbf{C}_{std}^X(s_1, s_2) = \sum_{i=1}^{\infty} \lambda_i^X \boldsymbol{\psi}_i^X(s_1)\, \boldsymbol{\psi}_i^X(s_2)^T$, for $s_1, s_2 \in \mathcal{S}$, where $\{\boldsymbol{\psi}_i^X\}$ are the orthonormal (i.e., $\langle \boldsymbol{\psi}_i^X, \boldsymbol{\psi}_j^X \rangle_{\mathbb{H}^X} = \delta_{ij}$, with δ_{ij} the Kronecker delta) multivariate eigenfunctions of $\mathbf{C}_{std}^X$ corresponding to the eigenvalues $\{\lambda_i^X\}$ in descending

order. Similarly, we consider for C^Y_{std} the expansion $C^Y_{std}(t_1,t_2) = \sum_{i=1}^{\infty} \lambda_i^Y \psi_i^Y(t_1)\,\psi_i^Y(t_2)$, for $t_1, t_2 \in \mathcal{T}$ where $\{\lambda_i^Y\}$ and $\{\psi_i^Y\}$ are defined in the same way. Note that both expansions are well defined in virtue of the multivariate and univariate versions of the Mercer's Theorem (Happ and Greven, 2018), respectively.

2.1 The Model

For the MFLR model we assume that the covariates $\mathbf{X}^{std}$ linearly influence the response Y^{std} as follows

$$Y^{std}(t) = \int_{\mathcal{S}} (\boldsymbol{\beta}(s,t))^T \mathbf{X}^{std}(s)\,ds + \varepsilon(t) \quad t \in \mathcal{T}, \tag{3}$$

that is a particular version of Equation (1). The regression coefficient vector $\boldsymbol{\beta} = (\beta_1, \ldots, \beta_p)^T$, is in $(L^2(\mathcal{S}\times\mathcal{T}))^p$, whose elements are vectors of bivariate functions in $L^2(\mathcal{S}\times\mathcal{T})$ (i.e., the space of square integrable function on the closed interval $\mathcal{S}\times\mathcal{T}$), and the random error function ε has $\mathrm{E}(\varepsilon) = 0$ and $\mathrm{Var}(\varepsilon) = v_\varepsilon^2$, and is independent of $\mathbf{X}^{std}$. Thus, the regression function is

$$\mathrm{E}\left(Y^{std}(t)\,|\mathbf{X}^{std}\right) = \int_{\mathcal{S}} (\boldsymbol{\beta}(s,t))^T \mathbf{X}^{std}(s)\,ds \quad t \in \mathcal{T}. \tag{4}$$

2.2 The Estimation Method

From the multivariate and univariate Karhunen-Loève's Theorem (Happ and Greven, 2018), standardized covariate and response variables can be represented as follows

$$\mathbf{X}^{std} = \sum_{i=1}^{\infty} \xi_i^X \boldsymbol{\psi}_i^X \quad Y^{std} = \sum_{i=1}^{\infty} \xi_i^Y \psi_i^Y, \tag{5}$$

where $\xi_i^X = \langle \mathbf{X}^{std}, \boldsymbol{\psi}_i^X \rangle_{\mathbb{H}^X}$ and $\xi_i^Y = \langle Y^{std}, \psi_i^Y \rangle$ are random variables, said *principal component scores* or simply *scores*, such that $\mathrm{E}\left(\xi_i^X\right) = 0$, $\mathrm{E}\left(\xi_i^X \xi_j^X\right) = \lambda_i^X \delta_{ij}$ and $\mathrm{E}\left(\xi_i^Y\right) = 0$, $\mathrm{E}\left(\xi_i^Y \xi_j^Y\right) = \lambda_i^Y \delta_{ij}$, respectively. In this context, the eigenfunctions $\{\boldsymbol{\psi}_i^X\}$ and $\{\psi_i^Y\}$ (as defined in the preliminaries) are referred to as *principal components* as well. As demonstrated

in Chiou et al. (2016), the regression coefficient vector is as follows

$$\boldsymbol{\beta}(s,t) = \sum_{i,j=1}^{\infty} \frac{\mathrm{E}\left(\xi_i^X \xi_j^Y\right)}{\lambda_i^X} \boldsymbol{\psi}_i^X(s)\, \psi_j^Y(t) \quad s \in \mathcal{S}, t \in \mathcal{T}, \tag{6}$$

which is also the minimizer of the expected squared $L^2(\mathcal{T})$ distance between Y^{std} and $\int_{\mathcal{S}} (\boldsymbol{f}(s,\cdot))^T \mathbf{X}^{std}(s)\, ds$, with $\boldsymbol{f} \in (L^2(\mathcal{S}\times\mathcal{T}))^p$, i.e.

$$\boldsymbol{\beta} = \underset{\boldsymbol{f}\in(L^2(\mathcal{S}\times\mathcal{T}))^p}{\operatorname{argmin}} \mathrm{E}\|Y^{std} - \int_{\mathcal{S}} (\boldsymbol{f}(s,\cdot))^T \mathbf{X}^{std}(s)\, ds\|^2. \tag{7}$$

By plugging Equation (5) and Equation (6) into Equation (4), and using the orthonormality of $\{\boldsymbol{\psi}_i^X\}$, we obtain

$$\mathrm{E}\left(Y^{std}(t)\,|\mathbf{X}^{std}\right) = \sum_{i,j=1}^{\infty} b_{ij} \xi_i^X \psi_j^Y(t) \quad t \in \mathcal{T}, \tag{8}$$

where $b_{ij} = \mathrm{E}\left(\xi_i^X \xi_j^Y\right)/\lambda_i^X$. Therefore, the best least squares predictor of Y given $\boldsymbol{X}$ is

$$\mathrm{E}(Y(t)\,|\mathbf{X}) = \mu^Y(t) + v^Y(t)^{1/2} E\left(Y^{std}(t)\,|\mathbf{X}^{std}\right) \quad t \in \mathcal{T}. \tag{9}$$

An estimation method of the above unknown quantities is described in the Supplementary Materials. Broadly speaking, it is based on the truncated versions of Equation (5), namely

$$\mathbf{X}_L^{std} = \sum_{i=1}^{L} \xi_i^X \boldsymbol{\psi}_i^X \quad Y_M^{std} = \sum_{i=1}^{M} \xi_i^Y \psi_i^Y, \tag{10}$$

where the number of retained scores L and M are chosen such that they explain at least given proportions $\delta_{\boldsymbol{X}}$ and δ_Y of total variation respectively (Ramsay, 2005). The estimation method provides estimators $\hat{\boldsymbol{\beta}}_{LM}$ of $\boldsymbol{\beta}$, in Equation (3), and $\hat{Y}_{LM}^{std}$ of $\mathrm{E}\left(Y^{std}|\mathbf{X}^{std}\right)$, in Equation (8), through the estimators $\hat{\boldsymbol{C}}_{std}^X$ and $\hat{C}_{std}^Y$ of $\boldsymbol{C}_{std}^X$ and C_{std}^Y calculated using the sample mean and covariance functions (Hsing and Eubank, 2015).

2.3 The Monitoring Strategy

Upon using the estimator $\hat{Y}_{LM}^{std}$, the functional residual in Equation (2) particularizes as

$$e^{std} = Y^{std} - \hat{Y}_{LM}^{std}. \tag{11}$$

To monitor the residuals, we follow the strategy of Woodall et al. (2004); Noorossana et al. (2012); Grasso et al. (2016); Pini et al. (2018). In particular, the *Hotelling*'s T^2 and the SPE control charts are applied on the coefficients obtained from the univariate functional principal component decomposition (Hsing and Eubank, 2015) of e^{std}, i.e.,

$$e^{std} = \sum_{i=1}^{\infty} \xi_i^e \psi_i^e, \tag{12}$$

where the scores $\xi_i^e = \langle e^{std}, \psi_i^e \rangle$ and the principal components $\{\psi_i^e\}$ are the eigenfunctions corresponding to the eigenvalues $\{\lambda_i^e\}$ in descending order of the covariance function $C^e(t_1, t_2) = \mathrm{Cov}\left(e^{std}(t_1), e^{std}(t_2)\right)$, for $t_1, t_2 \in \mathcal{T}$. As a matter of fact, C^e is different from C_{std}^Y (and thus $\{\psi_i^Y\}$ from $\{\psi_i^e\}$), because the former refers to the distribution of Y^{std}, whereas the latter is related to the conditional distribution of Y^{std} given $\mathbf{X}^{std}$. A straightforward approximation of e^{std} can be thus obtained as

$$e_K^{std} = \sum_{i=1}^{K} \xi_i^e \psi_i^e, \tag{13}$$

where K is the number of retained scores.

The *Hotelling*'s statistic T^2 can be then particularized as follows

$$T_{e^{std}}^2 = \boldsymbol{\xi}^e \boldsymbol{\Sigma}_{\boldsymbol{\xi}^e}^{-1} \boldsymbol{\xi}^e, \tag{14}$$

where $\boldsymbol{\Sigma}_{\boldsymbol{\xi}^e} = \mathrm{diag}\left(\lambda_1^e, \ldots, \lambda_K^e\right)$ is the variance-covariance matrix of $\boldsymbol{\xi}^e = \left(\xi_1^e, \ldots, \xi_K^e\right)^T$. Note that $T_{e^{std}}^2$ is the standardized square distance of the projection of e^{std} from the origin of the space spanned by the principal components $\{\psi_i^e\}$. Analogously, changes along directions

orthogonal to the latter space are monitored by the statistic

$$SPE_{e^{std}} = \int_{\mathcal{T}} \left(e^{std}(t) - e_K^{std}(t)\right)^2 dt. \tag{15}$$

The design phase of the control charts (Phase I) can be performed by means of a set of n functional residuals e_i^{std}, $i = 1, \ldots, n$, obtained by n independent observations $(\boldsymbol{X}_i, Y_i)$ acquired under IC conditions. This phase involves the estimation of the MFLR model unknown parameters (Supplementary Materials), of the principal components $\{\psi_i^e\}$ and of the matrix $\boldsymbol{\Sigma}_{\xi^e}$ (calculated by means of the sample covariance) as well as the estimation of the control limits for both the the *Hotelling*'s T^2 and the SPE control charts, which can be obtained by means of $(1-\alpha^*)$ quantiles of the empirical distribution of the two statistics. Note that, to control the *family wise error rate* (FWER) in the strong sense (Lehmann and Romano, 2006), α^* is chosen by using the Šidák correction (Lehmann and Romano, 2006) $\alpha^* = 1 - (1-\alpha)^{1/2}$, where α is the overall Type I error. In the monitoring phase (Phase II), functional residuals of a new observation $(\boldsymbol{X}^*, Y^*)$ are calculated and an alarm signal is issued if at least one realization of the $T^2_{e^{std}}$ and $SPE_{e^{std}}$ statistics violates the control limits.

3 Performance Analysis

3.1 Data Generation

The overall performance of the proposed FRCC are evaluated by means of a Monte Carlo simulation. Profile patterns have been generated with signal and correlation structures similar to those in the real-case study presented in Section 4. Details about the data generation process are provided in the Supplementary Materials. The compact domains $\mathcal{S}$ and $\mathcal{T}$ are set, without loss of generality, equal to $[0, 1]$ and the number of covariates p is set equal to 3. Moreover, in this section, the data are generated with $R^2 = \int_{[0,1]} \frac{\mathrm{Var}\left(\mathrm{E}\left(Y^{std}(t)|\mathbf{X}^{std}\right)\right)}{\mathrm{Var}\left(Y^{std}(t)\right)} dt$ set equal to 0.97 (Yao et al., 2005b). Additional analysis at different values of R^2 are provided in the Supplementary Materials.

The mean functions $\boldsymbol{\mu}^X$ and μ^Y of the generated data are obtained through the following

reference model

$$\mu(z) = P(z) + r\sum_{i=1}^{I} g_i(z; m_i, s_i) \quad z \in [0,1], \tag{16}$$

where

$$P(z) = az^2 + bz + c \quad z \in [0,1], \tag{17}$$

a, b, c are real numbers, and the terms $g_i(z; m_i, s_i)$ are normal probability density functions having parameters m_i and s_i with values given in the Supplementary Materials. The right side term of Equation (16) is inspired by the data generation process proposed in Pini et al. (2018); Grasso et al. (2017).

The aim of the simulation is to asses the FRCC performance in identifying mean function shifts in the response in presence of

1. mean function shifts in Y conditional on $\boldsymbol{X}$, i.e. $\mathrm{E}(Y|\boldsymbol{X})$, resulting from changes in μ^Y;

2. mean function shifts in $\boldsymbol{X}$, i.e., $\mathrm{E}(\boldsymbol{X}) = \boldsymbol{\mu}^X$, and $\mathrm{E}(Y|\boldsymbol{X})$.

The types of shift are consistent with those of Shu et al. (2004) and Wade and Woodall (1993). Note from Equations (4) and (9) that shifts in $\mathrm{E}(Y|\boldsymbol{X})$ can result from changes in μ^Y and $\boldsymbol{\beta}$. However, the latter, in addition, can affect variability of the functional regression residuals as well. Because we are interested in the FRCC performance in identifying mean function shifts in the response, given that the variability of the residuals are assumed constant, then, only shifts caused by changes in μ^Y are considered.

The functional patterns with shift in the mean function are generated using the model in Equation (16) with P defined as follows

$$P(z) = (a + \delta_a) z^2 + (b + \delta_b) z + (c + \delta_c) \quad z \in [0,1], \tag{18}$$

where the real number δ_a, δ_b, and δ_c define the shift type. Without loss of generality δ_a, δ_b, and δ_c are set equal to a positive severity level d as reported in Table 1 where four different types of shift (namely A,B,C,D) in $\boldsymbol{\mu}^X$ and μ^Y are considered. Shift A is representative of a change in the mean function curvature, whereas shift B and C represent slope modification and translation of the profile pattern, respectively. Shift D consists of both curvature and

Table 1. Different types of shift in $\boldsymbol{\mu}^X$ and μ^Y.

Shift	δ_a	δ_b	δ_c
A	d	0	0
B	0	d	0
C	0	0	d
D	d	d	0

Table 2. Severity levels associated to each type of shift in μ^Y for Scenario 1 (a) and for Scenario 2 (b).

	Shift	Severity
μ^Y	A	$d \in \{0.5, 1.0, 1.5, 2.0\}$
	B	$d \in \{0.5, 1.0, 1.5, 2.0\}$
	C	$d \in \{0.5, 1.0, 1.5, 2.0\}$
	D	$d \in \{0.5, 1.0, 1.5, 2.0\}$

(a)

	Shift	Severity		Shift	Severity
μ^Y	A	$d \in \{0.5, 1.0, 1.5, 2.0\}$	μ_1^X	D	$d \in \{0.5\}$
			μ_2^X	A	$d \in \{0.5\}$
			μ_3^X	D	$d \in \{1.0\}$

(b)

slope modifications of the mean function. These types of shift are indeed consistent with the real-case study of Section 4 and apt to model usual ways as ship performance increase or decrease in reality.

3.2 Simulation Results and Discussion

Three different profile monitoring methods are compared: (a) monitoring residuals by means of the FRCC, (b) monitoring model coefficients of the response variable Y via a *Hotelling*'s T^2 and SPE control charts (hereinafter denoted by RESP -RESPonse- control chart), and (c) monitoring the area under the response variable Y considered also in Pini et al. (2018) (hereinafter denoted by INBA -INdex BAsed- control chart).

Performance analysis of the FRCC is carried out by considering shifts in the conditional mean $\mathrm{E}(Y|\boldsymbol{X})$, firstly, by means of changes in μ^Y only (Scenario 1), and secondly by means of changes in both μ^Y and $\boldsymbol{\mu}^X$ (Scenario 2). The first scenario aims to analyse FRCC performance in absence of shift in the regressor mean $\boldsymbol{\mu}^X$; whereas, the second aims to study the unwanted influence of shifts in $\boldsymbol{\mu}^X$ on the FRCC performance. Severity levels and types of shift considered by Scenario 1 and Scenario 2 are listed in Table 2a and Table 2b, respectively. Note that in Scenario 2 we consider only shift type A (with the same severity levels of Scenario 1) for μ^Y, shift type D for μ_1^X, μ_3^X, and shift type A for μ_2^X. The latter three shifts are explored at only one severity level d as reported in Table 2b. For each shift type and severity level for Scenario 1 and for each severity level combination for Scenario 2, 100 simulation runs were performed. Each run consists of the following steps:

Phase I) A design set of 4000 IC patterns is randomly generated. In particular, $N_1 = 1000$ patterns form the training set are used to estimate MFLR model unknown quantities along with mean and covariance functions. The remaining $N_2 = 3000$ IC profiles are used as tuning set to estimate the empirical quantiles via the kernel density estimation (KDE) approach (Chou et al., 2001) with gaussian kernel, 2000 equally spaced points and bandwidth chosen by means of the Silverman's rule of thumb (Silverman, 1986). The number of retained scores L, M and K in Equation (10) and Equation (13) are chosen such that the retained principal components explain at least 95% of the total variability.

Phase II) A testing set of further 4000 OC patterns is randomly generated to carry out the monitoring phase and to evaluate the chart performance.

As is usually done in the literature (Montgomery, 2007), the FRCC and the competitor chart performance are compared by means of the average run length (ARL), that is referred to as ARL_0 in the case of no response mean shift ($d = 0$ for μ^Y), and as ARL_1 otherwise. For the sake of simplicity, we set $\text{ARL}_0 = 100$ and denote indistinctly by $\widehat{\text{ARL}}$ the estimated ARL (regardless whether it is referred to ARL_0 or ARL_1).

For Scenario 1, Table 3 shows the $\widehat{\text{ARL}}$s along with 95% approximate confidence intervals based on the Student's t approximation. Graphical representation of the latter are in Figure 1, which shows that the FRCC outperforms the RESP and INBA control charts for all the considered shifts. The gain in efficiency is less evident for Shift C (i.e., in presence of translations of the profile pattern, only) at high severity level ($d = 2$). Whereas, in Scenario 2, Table 4 and Figure 2 point out that shifts in covariate mean functions strongly impact the ARL of the FRCC. Indeed, when the response variable is IC ($d = 0$), $\widehat{\text{ARL}}$s for the FRCC are usually lower than $\text{ARL}_0 = 100$. Table 4 shows that this issue occurs to both the RESP and INBA control charts as well. For the latter charts this is expected because they do not account for the correlation between covariates and the response variable. On the contrary, this is not intuitive for the FRCC because it is expected not to be sensitive to unusual covariate realizations. However, this is completely consistent with what happens in the multivariate case (Shu et al., 2004). Indeed, let us denote with Δ^Y, Δ^{X_1}, Δ^{X_2} and Δ^{X_3} the shift size of Y, X_1, X_2 and X_3 means, respectively. Moreover, Y^{std} and $\boldsymbol{X}^{std}$

Table 3. Estimated ARLs ($\widehat{\text{ARL}}$s) and 95% confidence intervals (CI) for Scenario 1.

Shift	Severity	FRCC		RESP		INBA	
	d	$\widehat{\text{ARL}}$	CI	$\widehat{\text{ARL}}$	CI	$\widehat{\text{ARL}}$	CI
In-control	-	102.94	[97.95, 107.94]	100.81	[95.86, 105.76]	100.74	[97.81, 103.68]
A	0.5	62.14	[59.29, 64.98]	97.47	[92.37, 102.57]	100.03	[96.52, 103.53]
	1.0	20.43	[19.76, 21.10]	86.17	[82.21, 90.14]	91.85	[88.36, 95.34]
	1.5	6.94	[6.73, 7.14]	69.50	[66.80, 72.20]	73.44	[71.07, 75.80]
	2.0	2.93	[2.87, 2.99]	55.57	[53.26, 57.88]	62.59	[60.51, 64.67]
B	0.5	47.00	[45.02, 48.99]	98.65	[93.08, 104.22]	94.68	[91.16, 98.21]
	1.0	10.58	[10.18, 10.98]	82.10	[78.07, 86.13]	74.71	[72.38, 77.04]
	1.5	3.19	[3.11, 3.27]	68.97	[65.48, 72.45]	55.19	[53.31, 57.07]
	2.0	1.56	[1.54, 1.58]	52.78	[50.49, 55.08]	39.25	[38.18, 40.31]
C	0.5	8.30	[8.07, 8.54]	61.82	[59.56, 64.09]	74.51	[71.90, 77.12]
	1.0	1.33	[1.32, 1.34]	25.13	[24.20, 26.06]	39.03	[38.12, 39.95]
	1.5	1.00	[1.00, 1.00]	10.89	[10.52, 11.26]	20.82	[20.36, 21.27]
	2.0	1.00	[1.00, 1.00]	4.93	[4.81, 5.06]	11.48	[11.29, 11.67]
D	0.5	15.42	[14.89, 15.94]	87.00	[83.54, 90.47]	84.08	[80.77, 87.39]
	1.0	2.09	[2.06, 2.12]	56.50	[53.82, 59.18]	50.19	[48.53, 51.86]
	1.5	1.07	[1.07, 1.08]	32.38	[31.16, 33.60]	28.61	[27.99, 29.23]
	2.0	1.00	[1.00, 1.00]	19.37	[18.65, 20.08]	16.93	[16.64, 17.23]

Table 4. Estimated ARLs ($\widehat{\text{ARL}}$) and 95% confidence intervals (CI) for the FRCC in Scenario 2 at different severity levels d of shifts in the response mean (μ^Y) (Table 2b) as a function of which and how many covariates are subject to mean shift (each at the severity level reported in Table 2b). Zeros and ones in the triplets $(000, 100, 010, 001, 110, 101, 011, 111)$ indicate IC and OC covariates, respectively. For instance, the triplet 100 means that only the first covariate is OC, 111 means that all the covariates are OC, and so on.

μ^Y		FRCC		RESP		INBA	
d	shifted covariate combination	$\widehat{\text{ARL}}$	CI	$\widehat{\text{ARL}}$	CI	$\widehat{\text{ARL}}$	CI
0	0 0 0	99.79	[95.42, 104.17]	105.07	[99.21, 110.93]	104.19	[100.32, 108.05]
	1 0 0	78.09	[74.65, 81.53]	89.28	[85.67, 92.90]	100.1	[95.73, 104.48]
	0 1 0	100.61	[95.74, 105.49]	88.02	[84.26, 91.77]	79.51	[76.60, 82.41]
	0 0 1	100.59	[96.22, 104.97]	99.58	[94.68, 104.48]	102.34	[98.62, 106.05]
	1 1 0	73.43	[70.03, 76.84]	66.59	[63.48, 69.71]	93.63	[90.52, 96.75]
	1 0 1	64.73	[62.41, 67.05]	96.74	[92.93, 100.56]	99.88	[96.30, 103.45]
	0 1 1	97.21	[92.56, 101.86]	89.87	[85.42, 94.33]	80.11	[77.25, 82.98]
	1 1 1	63.26	[60.72, 65.8]	80.75	[76.73, 84.77]	92.93	[89.57, 96.29]
0.5	0 0 0	63.65	[60.80, 66.50]	105.16	[99.96, 110.37]	101.95	[98.24, 105.66]
	1 0 0	44.65	[43.18, 46.11]	85.52	[81.62, 89.41]	85.17	[82.11, 88.24]
	0 1 0	62.50	[59.69, 65.31]	96.76	[91.19, 102.32]	98.52	[95.03, 102.00]
	0 0 1	57.61	[55.37, 59.84]	97.09	[92.40, 101.79]	100.44	[96.94, 103.93]
	1 1 0	45.68	[43.87, 47.49]	77.36	[73.17, 81.56]	100.75	[96.94, 104.56]
	1 0 1	39.19	[37.58, 40.80]	94.04	[89.26, 98.82]	89.21	[86.48, 91.94]
	0 1 1	59.47	[56.76, 62.17]	96.78	[92.13, 101.42]	91.13	[87.46, 94.80]
	1 1 1	38.89	[37.34, 40.44]	84.76	[80.41, 89.11]	102.87	[98.66, 107.08]
1.0	0 0 0	21.08	[20.26, 21.90]	85.43	[81.25, 89.61]	89.22	[86.16, 92.28]
	1 0 0	17.23	[16.73, 17.74]	77.09	[73.45, 80.73]	69.95	[67.71, 72.19]
	0 1 0	21.18	[20.32, 22.04]	99.23	[94.10, 104.36]	102.16	[98.34, 105.97]
	0 0 1	20.28	[19.45, 21.11]	80.57	[76.86, 84.28]	91.30	[88.00, 94.60]
	1 1 0	17.68	[17.08, 18.27]	80.68	[76.93, 84.43]	99.91	[96.41, 103.41]
	1 0 1	16.41	[15.89, 16.93]	81.56	[77.90, 85.22]	77.33	[74.69, 79.97]
	0 1 1	20.64	[19.82, 21.45]	96.69	[92.09, 101.29]	98.09	[94.38, 101.81]
	1 1 1	16.53	[15.92, 17.14]	89.58	[84.46, 94.71]	100.85	[96.47, 105.22]
1.5	0 0 0	6.90	[6.70, 7.09]	69.54	[66.41, 72.67]	76.22	[73.66, 78.78]
	1 0 0	6.31	[6.14, 6.48]	68.29	[64.69, 71.89]	59.58	[57.74, 61.42]
	0 1 0	7.15	[6.91, 7.40]	91.92	[87.36, 96.47]	102.86	[98.68, 107.03]
	0 0 1	6.78	[6.58, 6.99]	66.91	[64.08, 69.75]	78.76	[76.14, 81.37]
	1 1 0	6.69	[6.50, 6.87]	76.35	[72.85, 79.84]	92.75	[89.30, 96.20]
	1 0 1	6.05	[5.89, 6.22]	66.45	[63.77, 69.12]	61.33	[59.57, 63.10]
	0 1 1	7.04	[6.83, 7.25]	86.49	[82.15, 90.84]	103.80	[99.44, 108.16]
	1 1 1	6.32	[6.12, 6.53]	80.95	[77.09, 84.82]	96.19	[92.72, 99.66]
2.0	0 0 0	2.92	[2.86, 2.98]	54.72	[52.55, 56.89]	63.70	[61.61, 65.80]
	1 0 0	2.83	[2.77, 2.89]	53.80	[51.71, 55.90]	48.41	[47.12, 49.71]
	0 1 0	3.01	[2.94, 3.08]	73.53	[70.12, 76.94]	96.58	[92.72, 100.43]
	0 0 1	2.90	[2.84, 2.96]	55.65	[53.00, 58.30]	66.34	[64.11, 68.57]
	1 1 0	2.86	[2.80, 2.92]	66.80	[63.87, 69.73]	80.97	[78.51, 83.43]
	1 0 1	2.76	[2.71, 2.81]	53.47	[51.42, 55.52]	50.93	[49.48, 52.39]
	0 1 1	2.94	[2.88, 3.00]	76.18	[72.50, 79.86]	99.79	[95.80, 103.77]
	1 1 1	2.77	[2.71, 2.83]	68.11	[64.88, 71.35]	82.87	[80.14, 85.61]

Figure 1. Estimated ARLs ($\widehat{\text{ARL}}$) and 95% confidence intervals for different response mean shifts for Scenario 1 (Table 3).

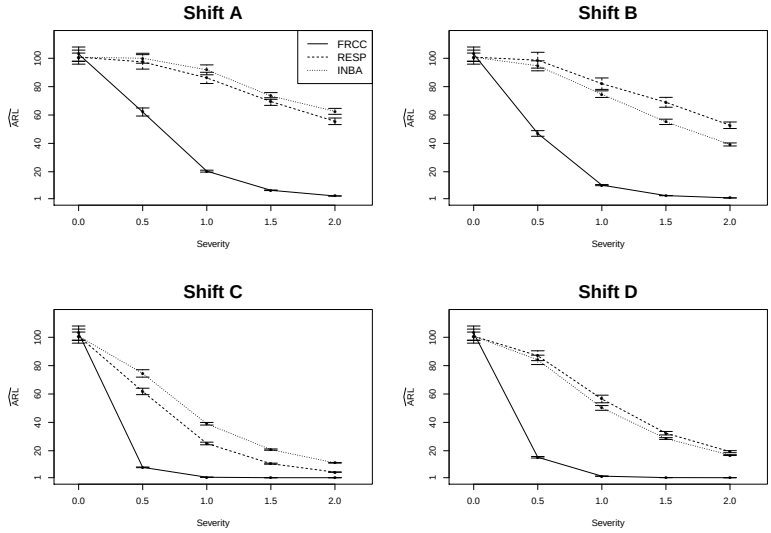

(resp. Y_{Δ}^{std} and $\boldsymbol{X}_{\Delta}^{std}$) indicate the standardized response and predictors in absence (resp. presence) of shift. Then, when mean shifts in both response variable and covariates occur, the functional residual (Equation (11)) can be rewritten, for $t \in [0,1]$, as

$$\begin{aligned} e_{\Delta}^{std}(t) &= Y_{\Delta}^{std}(t) - \hat{Y}_{LM\Delta}^{std}(t) \\ &= Y^{std}(t) + \int_0^1 \left(\boldsymbol{\beta}(s,t)\right)^T \mathbf{V}^X(s)^{-1} \boldsymbol{\Delta}^{\boldsymbol{X}}(s)\, ds + \frac{\Delta^Y(t)}{v^Y(t)^{1/2}} - \hat{Y}_{LM\Delta}^{std}(t) \\ &\quad - \int_0^1 \left(\hat{\boldsymbol{\beta}}_{LM}(s,t)\right)^T \mathbf{V}^X(s)^{-1} \boldsymbol{\Delta}^{\boldsymbol{X}}(s)\, ds \\ &= e^{std}(t) + \frac{\Delta^Y(t)}{v^Y(t)^{1/2}} - \int_0^1 \left(\boldsymbol{\beta}(s,t) - \hat{\boldsymbol{\beta}}_{LM}(s,t)\right)^T \mathbf{V}^X(s)^{-1} \boldsymbol{\Delta}^{\boldsymbol{X}}(s)\, ds, \end{aligned} \tag{19}$$

where e^{std} is as in Equation (11), $\hat{\boldsymbol{\beta}}_{LM}$ is the estimator of $\boldsymbol{\beta}$ given in the Supplementary Materials and $\mathbf{V}^X$ is defined in Section 2 with $p = 3$, $\boldsymbol{\Delta}^{\boldsymbol{X}} = \left(\Delta^{X_1}, \Delta^{X_2}, \Delta^{X_3}\right)^T$ and

$$\hat{Y}_{LM\Delta}^{std}(t) = \int_0^1 \left(\hat{\boldsymbol{\beta}}_{LM}(s,t)\right)^T \boldsymbol{X}_{\Delta}^{std}(s)\, ds \quad t \in [0,1]. \tag{20}$$

Then expected value of e_{Δ}^{std} conditioned on $\hat{\boldsymbol{\beta}}_{LM}$ is

$$\mathrm{E}\left(e_{\Delta}^{std}(t)\right) = \frac{\Delta^Y(t)}{v^Y(t)^{1/2}} - \int_0^1 \left(\boldsymbol{\beta}(s,t) - \hat{\boldsymbol{\beta}}_{LM}(s,t)\right)^T \mathbf{V}^X(s)^{-1} \boldsymbol{\Delta}^{\boldsymbol{X}}(s)\, ds \qquad t \in [0,1]. \tag{21}$$

Table 5. Estimation error magnitude of the entries of the coefficient vector $\boldsymbol{\beta}$

	X_1^{std}	X_2^{std}	X_3^{std}
Error	0.086	0.009	0.010

From Equation (19), it is clear that a mean shift in the residual, caused by covariate mean shifts ($\boldsymbol{\Delta^X} \neq 0$), occurs when the difference $\boldsymbol{\beta} - \hat{\boldsymbol{\beta}}_{LM}$ is not negligible, even though the response variable is IC, i.e., $\Delta^Y = 0$.

Figure 2. Estimated *ARL*s ($\widehat{\text{ARL}}$s) and 95% confidence intervals for the FRCC in Scenario 2 at different severity levels $d = \{0, 0.5, 1\}$ of shifts in the response mean (μ^Y) (Table 2b) as a function of which and how many covariates are subject to mean shift (each at the severity level reported in Table 2b). Zeros and ones in the triplets $(000, 100, 010, 001, 110, 101, 011, 111)$ indicate IC and OC covariates, respectively. For instance, the triplet 100 means that only the first covariate is OC, 111 means that all the covariates are OC, and so on. The severity levels $d = \{1.5, 2\}$ are not reported because the $\widehat{\text{ARL}}$s are all very small. The Figure depicts part of the results reported in Table 4.

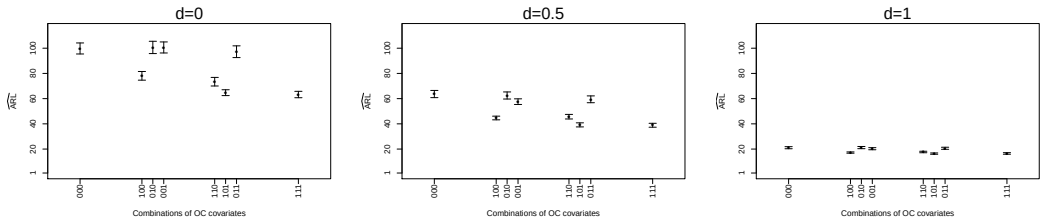

From Figure 2 and Table 4, it is clear that the magnitude of the deviations depends both on the number of covariates with shift in the mean function and the estimation error magnitude of the entries of the coefficient vector $\boldsymbol{\beta}$ in Table 5. The latter is measured as the L_2 distance between $\boldsymbol{\beta}$ and $\hat{\boldsymbol{\beta}}_{LM}$, estimated by means of 50 random realization of $\hat{\boldsymbol{\beta}}_{LM}$. Therefore, shifts in μ_1^X affect the performance of the FRCC stronger than mean shifts in the other covariates (viz. μ_2^X and μ_3^X). Obviously, this effect is more evident when the term $\frac{\Delta^Y}{(v^Y)^{1/2}}$ in Equation (19) is zero and do not cover the contribution to e_Δ^{std} of $\boldsymbol{\beta} - \hat{\boldsymbol{\beta}}_{LM}$. The problem of issuing an alarm only when a mean shift occurs in the response variable regardless of covariate mean shifts is addressed in Section 3.3 and solutions are proposed in this respect.

3.3 Remarks on the Use of the FRCC in Presence of Covariate Mean shifts

As stated before, the FRCC performance in identifying OC condition (of the response variable) can be affected by the number of covariates with shift in the mean function and

the estimation error of the coefficient vector $\boldsymbol{\beta}$ (Table 4). In particular, when mean shifts occur in the covariates only, the interpretation of the FRCC becomes cumbersome, because a point falling outside the FRCC control limits is wrongly assigned to a shift in the response variable. In this section, we propose some solutions to enhance the FRCC performance in presence of covariate mean shifts.

As pointed out in Scenario 1 of the simulation study (Table 2a), which assumes no covariate mean shift, the FRCC performance in identifying response mean shifts is always better than that achieved by the competitor control charts (Figure 1). A straightforward solution is to verify the assumption that no covariate mean shift occurs by extending to the functional setting the control charts proposed by Wade and Woodall (1993) in the multivariate case. In this regard, Capezza et al. (2019) suggest to monitor the covariates $\mathbf{X}$ through the jointly use of the *Hotelling*'s T^2 and SPE control charts built on the principal component decomposition of $\mathbf{X}^{std}$.

When the number of observations available in Phase I, N_1, is large, an alternative solution, which does not the construction of additional control charts, can be based on the consistency of the estimator $\hat{\boldsymbol{\beta}}_{LM}$ of the coefficient vector $\boldsymbol{\beta}$ (Chiou et al., 2016). Indeed, when truncation parameters L and M in Equation (10) go to infinity with N_1, the impact of $\boldsymbol{\Delta}^{\boldsymbol{X}}$ in Equation (19) and (21) fades out, as in (Yao et al., 2005b), even though they do not provide more detailed indications on the convergence rate. That is

$$\lim_{N_1 \to \infty} \int_{\mathcal{S}} \int_{\mathcal{T}} \left[\boldsymbol{\beta}(s,t) - \hat{\boldsymbol{\beta}}_{LM}(s,t) \right]^2 ds dt = 0 \quad \textit{in probability.} \tag{22}$$

This result indicates that, theoretically, for large N_1, L and M can be increased in order to ensure convergence. In this perspective, we perform again the simulations in Scenario 2 (that assumes covariate mean shifts reported in Table 2b in the case of no response mean shifts ($d = 0$ for μ^Y)) with $L = 5, 10, 20$ and $M = 2, 3, 4$. The results are shown in Figure 3, where $\widehat{\text{ARL}}$s (which is in this case estimating $\text{ARL}_0 = 100$) in function of the number of covariates with shift in the mean function (according to Table 4) are reported by varying L (row-wise) and M (column-wise). Comparing these results with the top-left panel of Figure 2 ($d = 0$), it is clear that the negative effect (i.e., $\widehat{\text{ARL}}$ not equal to $\text{ARL}_0 = 100$) caused by covariate mean shifts are attenuated by choosing L and M as large as possible

Figure 3. Estimated *ARL*s ($\widehat{\text{ARL}}$) and 95% confidence intervals for the FRCC in Scenario 2 no shift ($d = 0$) in the response mean (μ^Y) at different values of truncation parameters L (increasing from top to bottom panel) and M (increasing from left to right panel) as a function of which and how many covariates are OC (each at the severity level reported in Table 2b). Zeros and ones in the triplets $(000, 100, 010, 001, 110, 101, 011, 111)$ indicate IC and OC covariates, respectively. For instance, the triplet 100 means that the first covariate mean has shifted, 111 means that all the covariate mean are shifted, and so on.

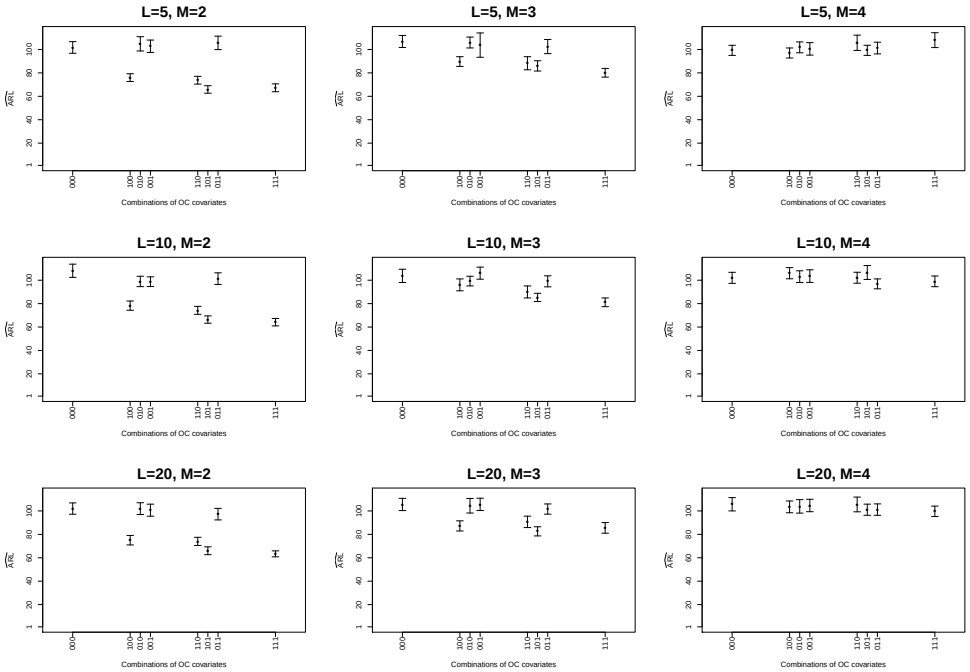

(see the bottom-right panel of Figure 3). In general, the latter recommendation is expected to attenuate the effect on $\widehat{\text{ARL}}$ of the covariate mean shifts, when there is a shift also in the response mean (depicted in panels $d = 0.5, 1.0, 1.5, 2.0$ of Figure 2).

Otherwise, when N_1 is small, we propose to use in the monitoring strategy (Section 2.3) the following scaled functional residual (hereinafter referred to as *studentized residual*)

$$e_{stu}^{std}(t) = \frac{Y^{std}(t) - \hat{Y}_{LM}^{std}(t)}{\left(\hat{\sigma}_{\varepsilon}^2(t) + \hat{\omega}_{LM}(t,t)\right)^{1/2}} \quad t \in \mathcal{T}, \tag{23}$$

instead of that in Equation (11). In Equation (23), $\hat{\sigma}_{\varepsilon}^2$ is an estimator of $\text{Var}(\varepsilon)$ and $\hat{\omega}_{LM}$ is defined as

$$\hat{\omega}_{LM}(s,t) = \text{Cov}\left(\hat{Y}_{LM}^{std}(t) \,|\mathbf{X}^{std}\right) = \left(\hat{\boldsymbol{\xi}}_L^{\boldsymbol{X}}\right)^T \left(\hat{\boldsymbol{\Xi}}_{\boldsymbol{X}}^T \hat{\boldsymbol{\Xi}}_{\boldsymbol{X}}\right)^{-1} \hat{\boldsymbol{\xi}}_L^{\boldsymbol{X}} \hat{\boldsymbol{\psi}}_M^Y(s)^T \hat{\boldsymbol{\Sigma}}_{\boldsymbol{\epsilon}_M} \hat{\boldsymbol{\psi}}_M^Y(t) \quad s \in \mathcal{S}, t \in \mathcal{T}, \tag{24}$$

where $\hat{\boldsymbol{\xi}}_L^{\boldsymbol{X}}$ is the estimator of the score vector $\boldsymbol{\xi}_L^X$ of $\mathbf{X}^{std}$, $\hat{\boldsymbol{\Xi}}_{\boldsymbol{X}}^T \hat{\boldsymbol{\Xi}}_{\boldsymbol{X}}$ is the estimator of $N_1 \,\text{Cov}\left(\boldsymbol{\xi}_L^X, \boldsymbol{\xi}_L^X\right)$, $\hat{\boldsymbol{\psi}}_M^Y$ is the estimator of the vector of the first M eigenfunctions of Y^{std},

and $\hat{\boldsymbol{\Sigma}}_{\boldsymbol{\epsilon}_M}$ is the estimator of $\mathrm{Cov}(\boldsymbol{\epsilon}_M)$. Given e^{std}_{stu} in Equation (23), the *Hotelling*'s T^2 and SPE statistics, defined in Section 2.3, are particularized by the statistics $T^2_{e^{std}_{stu}}$ and $SPE_{e^{std}_{stu}}$ obtained by replacing e^{std} with e^{std}_{stu}, in Equation (14) and (15), respectively. This particular choice for the FRCC will be referred to as *studentized functional regression control chart* (sFRCC) which can be regarded as an extension to functional data of the regression control chart with prediction interval proposed by Wade and Woodall (1993). The studentized functional residual is the functional extension of the studentized residual that arises in the multivariate case (Woodall et al., 2004), with $\hat{\sigma}^2_{\varepsilon}(t)+\hat{\omega}_{LM}(t,t)$, for $t \in \mathcal{T}$, the variance function of e^{std}. The effect of $\hat{\sigma}^2_{\varepsilon}(t)+\hat{\omega}_{LM}(t,t)$, for $t \in \mathcal{T}$, on the latter is that of reducing the influence of covariate mean shifts on the residual mean. Indeed, the larger the term $\hat{\omega}_{LM}$, i.e., the more extreme realization of $\boldsymbol{X}^{std}$, the heavier the corresponding residual is rescaled and thus the higher the probability of the observation to be judged IC. And this is because the more the observations are far from the center of the sample cloud the larger the residual uncertainty. However, for a large N_1, consistently with the dataset complexity, the use of the sFRCC leads to the same results of the FRCC defined before, because in this case, $\hat{\omega}_{LM}(t,t)$, for $t \in \mathcal{T}$, tends to zero. Therefore, all the residuals are equally rescaled regardless of the values achieved by the covariates.

To investigate the performance of the sFRCC, we carry out again simulation in Scenario 2 only in the case of no response mean shift ($d = 0$ for μ^Y) by setting N_1 equal to 100 and 50. Results are reported in Figure 4 and show that $\widehat{\mathrm{ARL}}$s achieved by the sFRCC are closer to the true value ($\mathrm{ARL}_0 = 100$) than those obtained by means of the FRCC. In this simulation, the truncation parameters L, M and K in Equation (10) and Equation (13) shall be chosen large enough to avoid truncation bias, as addressed before, (in case of large N_1) but small enough to avoid overfitting problems due to small N_1. In this simulation, we found appropriate to choose L, M and K such that the retained principal components explain the 99% of total variation. Too small values of L, M and K would not highlight the benefit of the term $\hat{\omega}_{LM}(t,t)$, for $t \in \mathcal{T}$, in the studentized residuals of Equation (23). Therefore, as in the multivariate case studied by Woodall et al. (2004), also in the functional setting, the sFRCC is able to control the Type I error (i.e., $\mathrm{ARL}_0 = 100$) in case of covariate mean shifts. However, when the assumption of no covariate mean shift can be given as

Figure 4. Estimated *ARL*s ($\widehat{\text{ARL}}$s) and 95% confidence intervals for the FRCC (left column panels) and sFRCC (right column panels) in Scenario 2 no shift ($d = 0$) in the response mean (μ^Y) at different sample sizes $N_1 = 100, 50$ as a function of which and how many covariates are subject to mean shift (each at the severity level reported in Table 2b). Zeros and ones in the triplets $(000, 100, 010, 001, 110, 101, 011, 111)$ indicate IC and OC covariates, respectively. For instance, the triplet 100 means that only the first covariate is OC, 111 means that all the covariates are OC, and so on.

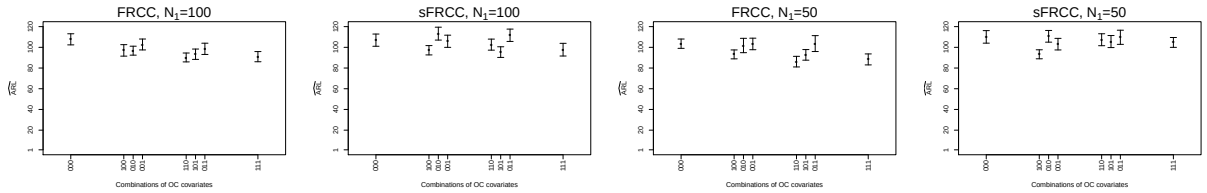

satisfied (e.g., for technological reasons), the FRCC is recommended since it results more sensitive than the sFRCC in detecting OC condition (of the functional response mean) as the latter has control limits wider than those of the FRCC.

4 Real-case Study: Fuel Consumption Monitoring in the Shipping Industry

To demonstrate the potential and the applicability of the proposed control chart in practical situations, a real-case study in the shipping industry is presented henceforth. It addresses the issue of monitoring ship fuel consumption and, thus, CO_2 emissions, which, in view of the dramatic climate change, is of great interest in the maritime field in the very last years. Indeed, the new Regulation (EU 2015/757) of the European Union (EU) Council of 25 April 2015, coherently with the previous guidelines of the International Maritime Organization (IMO), compel operators having ships sailing in the Mediterranean Sea to monitor, report and verify (MRV) CO_2 emissions. In account of this, shipping companies are nowadays setting-up multi-sensor systems for massive high frequency recordings of operational data to be available. A large portion of these is suitably modelled as functional data.

In this study, data recorded during 2015, 2016, and 2017 from a Ro-Pax ship (owned by the shipping company *Grimaldi Group*) are analysed. The total number of voyages is 315. During each voyage the Data AcQuisition (DAQ) device mounted on the ship have been collecting signals at five-minute frequency. The data refer only to the *navigation phase*, i.e., the time interval between the *finished with engine order* (when the ship leaves the departure port) and the *stand by engine order* (when the ship enters the arrival port). In particular,

the percentage of travelled distance over the voyage is chosen as functional domain so that variables coming from different voyages are defined on interval of the same width. The *cumulative fuel consumption* (CFC) per each voyage is assumed as the functional response variable. It is the cumulative sum of the fuel consumption during the navigation phase. The following set of covariates are assumed as influencing the response: *sailing time* (T), measured in hours (h), which is the cumulative navigation time during the navigation phase; *speed over ground* (SOG), measured in knots (kn), which is the ratio between the sailed distance over ground, i.e., the distance travelled by the vessel during the navigation, and the sailing time; *longitudinal* and *transverse wind components* (W_{lo} and W_{tr}), measured in knots (kn), which are functions of the true wind speed and the difference between the true wind angle (in the earth system) and the course over ground. Covariates are chosen on the basis of both engineering and statistical considerations. Additional information about the response and regressor variables can be found in Bocchetti et al. (2015); Erto et al. (2015). The 315 profiles observed for the response and covariates in the considered period are shown in the Supplementary Materials. Throughout February 2016, EEI (energy efficiency initiative) was performed on the considered ship, which mainly consisted in a silicone foul realising coat of the hull. As guranteed by the paint company, and described in Erto et al. (2015), this EEI plausibly produces a shift in the CFC mean. As shown in the Supplementary Materials, this is also confirmed by visual inspection of the mean function of the response before and after the EEI. In light of this, the 112 profiles relating to the period before dry-dock operations, are used to form the Phase I sample. Whereas, the remaining 203 profiles are used in Phase II to evaluate the proposed chart performance.

4.1 Implementation Details and Results

The Phase I sample consists of 112 profiles observed at five-minute frequency during each voyage. The functional observations are obtained by solving a regularization problem where profiles are approximated by means of a cubic *B-spline* basis expansion (i.e., of order 4) with 100 basis and 98 equispaced knots, and a smoothing parameter on the second derivative equal to 10^{-10}, chosen by means of generalized cross validation (Ramsay, 2005). Then, the IC observations are identified by extending the approach proposed by Colosimo and Pacella

Figure 5. $T^2_{e^{std}}$ and $SPE_{e^{std}}$ charts for the FRCC, the sFRCC, and, the RESP and INBA control charts. The vertical dotdash line corresponds to the last voyage before the EEI.

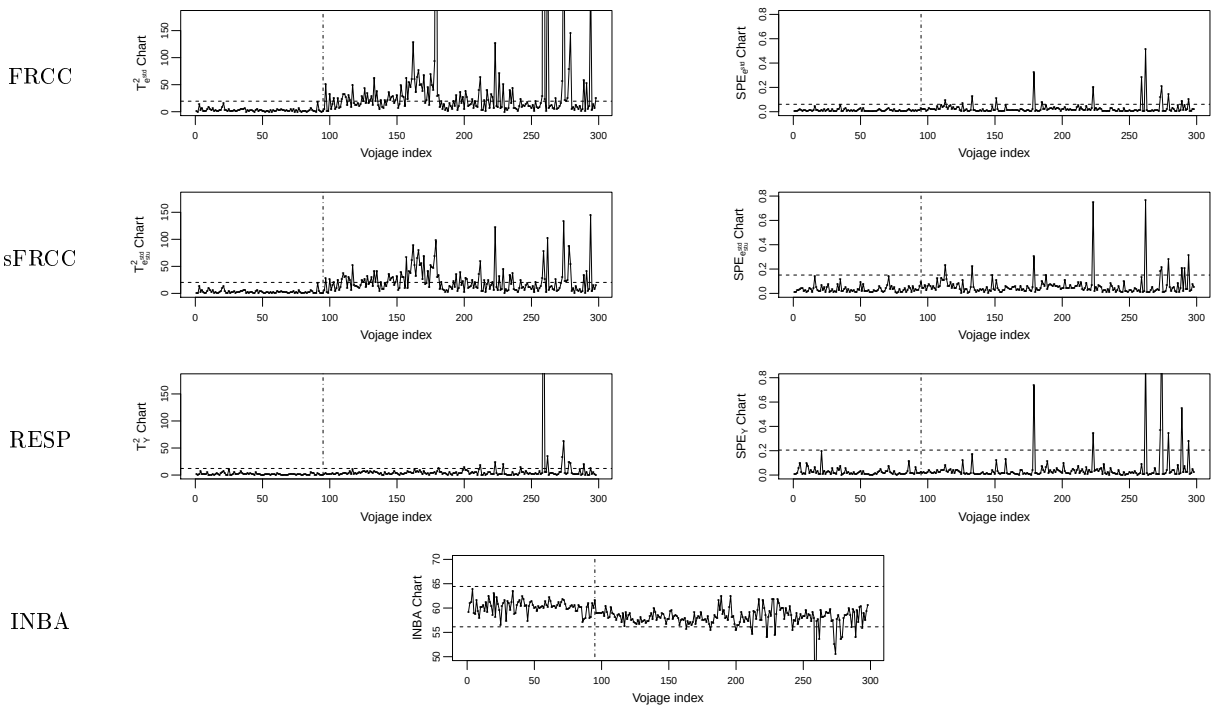

(2007) to the multivariate functional case. As in Section 3, the appropriate values of L, M and K in Equation (10) and Equation (13) are found as those for whichf the retained principal components explain at least 95% of total variation. Then, the control limits are estimated using the empirical quantiles of the T^2_e ans SPE^e distribution estimated through the KDE procedure, as in the simulation study (Section 3.2), with the overall Type I error α equal to 0.0027 (which corresponds to $\text{ARL}_0 = 370$). The choice of α is prompted by the common industrial practice in analogy with the classic Shewhart control chart with 3-sigma limits (Montgomery, 2007). The remaining 203 profiles used in Phase II are obtained in the same way as in Phase I. Even if the use of the sFRCC has been recommended in all cases (Section 3.3), for the sake of completeness both the FRCC and the sFRCC have been applied. Each observation is plotted onto those two control charts and the two competitor ones (RESP and INBA) as shown in Figure 5.

By comparing the four charts, the responsiveness of the FRCC and the sFRCC is evidently higher than that of the the INBA and the RESP control charts which signal a much lower number of OCs. In particular, in the FRCC and the sFRCC the change in the

Table 6. Estimated ARL ($\widehat{\text{ARL}}$), mean $\overline{\text{ARL}}^*$ of the empirical bootstrap *ARL* distribution, 95% confidence interval (*CI*) for the ARL statistic, and *p-values* of bootstrap test on the ARL mean differences for each chart combination.

	$\widehat{\text{ARL}}$	$\overline{\text{ARL}}^*$	*CI*	*p-value*			
				FRCC	sFRCC	RESP	INBA
FRCC	2.07	2.03	[1.78, 2.34]	-	-	-	-
sFRCC	2.11	2.21	[1.90, 2.56]	0.000999	-	-	-
RESP	9.46	10.09	[6.13, 17.92]	0.000999	0.000999	-	-
INBA	11.28	11.71	[7.81, 18.45]	0.000999	0.000999	0.000999	-

response mean is almost exclusively captured by the T^2 control chart, which means that dissimilarities between the Phase I and Phase II samples occur mostly in the space spanned by the retained principal components. As expected by remarks given in Section 3.3, Figure 5 shows that the sFRCC is less sensitive than the FRCC in detecting OC condition (of the functional response). However, the former chart should be used in this case because the assumption of no covariate mean shift cannot be given as satisfied. More precisely, by looking at the first column of Table 6, the estimated ARLs ($\widehat{\text{ARL}}$) achieved by FRCC and sFRCC are at least a fourth of those achieved by the RESP and INBA control charts.

To quantify the uncertainty of $\widehat{\text{ARL}}$s, a bootstrap analysis (Efron and Tibshirani, 1986) was performed (see Supplementary Materials for more details).

Table 6 shows the mean $\overline{\text{ARL}}^*$ of the empirical bootstrap *ARL* distribution and the bootstrap confidence intervals for each chart. Moreover, to test whether the mean of the empirical bootstrap *ARL* distributions differ significantly, bootstrap tests on the ARL mean differences (Efron and Tibshirani, 1986) for each chart combination were performed. The *p-values* are shown in Table 6 for each chart combination test. The bootstrap analysis, i.e., tests and confidence intervals, further confirms that both the FRCC and the sFRCC outperform the competitor control charts. Indeed, 95% confidence intervals are strictly below those of the RESP and INBA control charts and accordingly the tests reject the hypothesis of equal means for each chart combination.

Table 7 shows for the FRCC, sFRCC, and RESP control charts the estimated ARLs ($\widehat{\text{ARL}}$), the mean $\overline{\text{ARL}}^*$ of the empirical bootstrap *ARL* distribution and the bootstrap 95% confidence intervals at different δ_Y and $\delta_{\boldsymbol{X}}$ (i.e., percentages of variance explained by the retained scores in the response and covariates). The analysis for the INBA control charts is not influenced by different values of δ_Y and $\delta_{\boldsymbol{X}}$ and therefore, the results are equal to those already reported in Table 6. Results in Table 7 show that bot FRCC and sFRCC

Table 7. Estimated ARL ($\widehat{\text{ARL}}$), mean $\overline{\text{ARL}}^*$ of the empirical bootstrap *ARL* distribution, and 95% confidence interval (CI) for the ARL statistic at different δ_Y, and $\delta_{\boldsymbol{X}}$, for the FRCC, sFRCC and RESP control chart.

	δ_Y	0.95 ($M=2$)			0.98 ($M=3$)			0.99 ($M=5$)		
$\delta_{\boldsymbol{X}}$		$\widehat{\text{ARL}}$	$\overline{\text{ARL}}^*$	*CI*	$\widehat{\text{ARL}}$	$\overline{\text{ARL}}^*$	*CI*	$\widehat{\text{ARL}}$	$\overline{\text{ARL}}^*$	*CI*
0.90 ($L=19$)	FRCC	2.99	3.06	[2.51, 3.77]	1.97	2.00	[1.77, 2.31]	1.96	2.00	[1.74, 2.29]
	sFRCC	2.89	2.95	[2.46, 3.62]	2.19	2.20	[1.92, 2.55]	2.25	2.28	[1.94, 2.67]
	RESP	9.46	9.99	[6.23, 17.87]	9.08	9.72	[5.90, 17.95]	5.72	6.50	[2.12, 12.92]
0.95 ($L=36$)	FRCC	2.02	2.03	[1.76, 2.34]	1.66	1.67	[1.51, 1.87]	1.24	1.23	[1.17, 1.31]
	sFRCC	2.16	2.21	[1.90, 2.56]	1.71	1.72	[1.54, 1.94]	1.28	1.28	[1.21, 1.37]
	RESP	9.46	10.09	[6.13, 17.92]	9.08	9.45	[5.74, 16.55]	5.72	6.43	[2.41, 11.53]
0.97 ($L=56$)	FRCC	1.36	1.36	[1.26, 1.47]	1.27	1.26	[1.19, 1.34]	1.62	1.63	[1.46, 1.82]
	sFRCC	1.46	1.48	[1.36, 1.62]	1.42	1.43	[1.31, 1.57]	1.84	1.86	[1.64, 2.13]
	RESP	9.46	10.24	[6.05, 17.14]	9.08	9.60	[5.75, 17.16]	5.72	6.41	[2.39, 12.19]

outperform the competitor ones for all δ_Y and $\delta_{\boldsymbol{X}}$ values. However, as expected by remarks given in Section 3.3, the choice of the number L and M (Equation (10)) of the retained scores (related to δ_Y and $\delta_{\boldsymbol{X}}$) affects the performance of the FRCC and sFRCC.

5 Conclusions

In this paper, we propose a new general framework for monitoring a functional quality characteristic when functional covariates are available, referred to as *functional regression control chart* (FRCC). In particular, the quality characteristic is adjusted for the effects of the covariates by means of multivariate functional linear regression model and then monitored by using jointly the *Hotelling*'s T^2 and the SPE control charts built on its functional principal component decomposition. However the approach is very general, indeed the choice of the model, the estimation method as well as the monitoring strategy can be easily extended. To the best of the authors' knowledge, profile monitoring methods that are promptly able to enhance the monitoring by exploiting additional information on covariates (even possibly functional ones) are not present in the literature, whose attention is mainly focused on procedures that consider measurements of the functional quality characteristic only.

A Monte Carlo simulation is carried out with the aim of investigating the performance of the proposed control chart in identifying mean shifts in the response. The FRCC is then compared with other two control charts (named Response and INdex-BAsed control charts) that are widely used both in the literature and in real profile monitoring applications. The results showed that, firstly, the FRCC is far better than the competitor control charts

in identifying response mean shifts, when no covariate mean shift occurs; secondly, the covariate mean shift implies estimation error of the coefficient vector and thus, strongly affects FRCC performance in terms of average run length. When the assumption of no covariate mean shift cannot be given as satisfied, some solutions are proposed in case of both large and small Phase I sample sizes. In the latter case, a studentized version of the FRCC (sFRCC) is proposed to take into account the different residual variance at different covariate values. Eventually, by means of a real-case study in the shipping industry, the FRCC and sFRCC is shown to outperform the competitor control charts in identifying CO_2 emission reduction after a specific energy efficiency initiative.

Future researches can be addressed on extending the FRCC framework to different types of regression models and to different residual monitoring strategies. Moreover, the effect on the FRCC performance in detecting shifts in the variance function of both the response and covariates deserve further investigations.

Supplementary Materials

The Supplementary Materials contain the procedure to estimate the MFLR model, details on data generation in the simulation study, additional simulation for different values of R^2, the description of the bootstrap procedure used in the real-case study as well as figures showing the observed profiles.

References

Bocchetti, D., A. Lepore, B. Palumbo, and L. Vitiello (2015). A statistical approach to ship fuel consumption monitoring. *Journal of Ship Research 59*(3), 162–171.

Capezza, C., A. Lepore, A. Menafoglio, B. Palumbo, and S. Vantini (2019). Control charts for monitoring ship operating conditions and co_2 emissions based on scalar-on-function regression. *MOX–Report 12/2019*.

Cardot, H., F. Ferraty, and P. Sarda (2003). Spline estimators for the functional linear model. *Statistica Sinica 13*, 571–591.

Chiou, J.-M., Y.-T. Chen, and Y.-F. Yang (2014). Multivariate functional principal component analysis: A normalization approach. *Statistica Sinica*, 1571–1596.

Chiou, J.-M., Y.-F. Yang, and Y.-T. Chen (2016). Multivariate functional linear regression and prediction. *Journal of Multivariate Analysis 146*, 301–312.

Chou, Y.-M., R. L. Mason, and J. C. Young (2001). The control chart for individual observations from a multivariate non-normal distribution. *Communications in statistics-Theory and methods 30*(8-9), 1937–1949.

Colosimo, B. M. and M. Pacella (2007). On the use of principal component analysis to identify systematic patterns in roundness profiles. *Quality and reliability engineering international 23*(6), 707–725.

Colosimo, B. M. and M. Pacella (2010). A comparison study of control charts for statistical monitoring of functional data. *International Journal of Production Research 48*(6), 1575–1601.

Efron, B. and R. Tibshirani (1986). Bootstrap methods for standard errors, confidence intervals, and other measures of statistical accuracy. *Statistical Science 1*(1), 54–75.

Erto, P., A. Lepore, B. Palumbo, and L. Vitiello (2015). A procedure for predicting and controlling the ship fuel consumption: Its implementation and test. *Quality and Reliability Engineering International 31*(7), 1177–1184.

Fan, Y., N. Foutz, G. M. James, W. Jank, et al. (2014). Functional response additive model estimation with online virtual stock markets. *The Annals of Applied Statistics 8*(4), 2435–2460.

Ferraty, F. and P. Vieu (2006). *Nonparametric functional data analysis: theory and practice*. Springer Science & Business Media.

Grasso, M., B. M. Colosimo, and F. Tsung (2017). A phase i multi-modelling approach for profile monitoring of signal data. *International Journal of Production Research 55*(15), 4354–4377.

Grasso, M., A. Menafoglio, B. M. Colosimo, and P. Secchi (2016). Using curve-registration information for profile monitoring. *Journal of Quality Technology 48*(2), 99.

Hall, P., J. L. Horowitz, et al. (2007). Methodology and convergence rates for functional linear regression. *The Annals of Statistics 35*(1), 70–91.

Happ, C. and S. Greven (2018). Multivariate functional principal component analysis for data observed on different (dimensional) domains. *Journal of the American Statistical Association*, 1–11.

Hawkins, D. M. (1991). Multivariate quality control based on regression-adjusted variables. *Technometrics 33*(1), 61–75.

Hawkins, D. M. (1993). Regression adjustment for variables in multivariate quality control. *Journal of Quality Technology 25*(3), 170–182.

Hsing, T. and R. Eubank (2015). *Theoretical foundations of functional data analysis, with an introduction to linear operators*. John Wiley & Sons.

Jin, J. and J. Shi (1999). Feature-preserving data compression of stamping tonnage information using wavelets. *Technometrics 41*(4), 327–339.

Lehmann, E. L. and J. P. Romano (2006). *Testing statistical hypotheses*. Springer Science & Business Media.

Mandel, B. (1969). The regression control chart. *Journal of Quality Technology 1*(1), 1–9.

Matsui, H., S. Kawano, and S. Konishi (2009). Regularized functional regression modeling for functional response and predictors. *Journal of Math-for-industry 1*(3), 17–25.

Menafoglio, A., M. Grasso, P. Secchi, and B. M. Colosimo (2018). Profile monitoring of probability density functions via simplicial functional pca with application to image data. *Technometrics 60*(4), 497–510.

Montgomery, D. C. (2007). *Introduction to statistical quality control*. John Wiley & Sons.

Noorossana, R., A. Saghaei, and A. Amiri (2012). *Statistical analysis of profile monitoring*. John Wiley & Sons.

Pini, A., S. Vantini, B. M. Colosimo, and M. Grasso (2018). Domain-selective functional analysis of variance for supervised statistical profile monitoring of signal data. *Journal of the Royal Statistical Society: Series C (Applied Statistics) 67*(1), 55–81.

R Core Team (2018). *R: A Language and Environment for Statistical Computing*. Vienna, Austria: R Foundation for Statistical Computing.

Ramsay, J. O. (2005). *Functional data analysis*. Wiley Online Library.

Shu, L., F. Tsung, and T. Kwok-Leung (2004). Run-length performance of regression control charts with estimated parameters. *Journal of Quality Technology 36*(3), 280.

Silverman, B. W. (1986). *Density estimation for statistics and data analysis*, Volume 26. CRC press.

Wade, M. R. and W. H. Woodall (1993). A review and analysis of cause-selecting control charts. *Journal of quality technology 25*(3), 161–169.

Woodall, W. H., D. J. Spitzner, D. C. Montgomery, and S. Gupta (2004). Using control charts to monitor process and product quality profiles. *Journal of Quality Technology 36*(3), 309.

Yao, F., H.-G. Müller, and J.-L. Wang (2005a). Functional data analysis for sparse longitudinal data. *Journal of the American Statistical Association 100*(470), 577–590.

Yao, F., H.-G. Müller, and J.-L. Wang (2005b). Functional linear regression analysis for longitudinal data. *The Annals of Statistics*, 2873–2903.

Zhou, M. and T. Goh (2016). Effects of model accuracy on residual control charts. *Quality and Reliability Engineering International 32*(5), 1785–1794.

MOX Technical Reports, last issues

Dipartimento di Matematica
Politecnico di Milano, Via Bonardi 9 - 20133 Milano (Italy)

75/2020 F. Dassi; A. Fumagalli; D. Losapio; S. Scialò; A. Scotti; G. Vacca
The mixed virtual element method for grids with curved interfaces

74/2020 Formaggia, L; Fumagalli, A.; Scotti, A.
A multi-layer reactive transport model for fractured porous media

73/2020 Bennati, L.; Vergara, C.; Domanin, M.; Trimarchi, S.; Malloggi, C.; Silani, V.; Parati, G.; Casa
A computational fluid structure interaction study for carotids with different atherosclerotic plaques

72/2020 Belli E.; Vantini S.
Measure Inducing Classification and Regression Trees for Functional Data

71/2020 Belli E; Vantini S.
Ridge regression with adaptive additive rectangles and other piecewise functional templates

70/2020 Belli E.
Smoothly Adaptively Centered Ridge Estimator

69/2020 Galvani, M.; Torti, A.; Menafoglio, A.; Vantini S.
FunCC: a new bi-clustering algorithm for functional data with misalignment

67/2020 Caramenti, L.; Menafoglio, A.; Sgobba, S.; Lanzano, G.
Multi-Source Geographically Weighted Regression for Regionalized Ground-Motion Models

66/2020 Didkovsky, O.; Ivanov, V.; Papini, M.; Longoni, L.; Menafoglio, A.
A comparison between machine learning and functional geostatistics approaches for data-driven analyses of solid transport in a pre-Alpine stream

65/2020 Di Gregorio, S.; Vergara, C.; Montino Pelagi, G.; Baggiano, A.; Zunino, P.; Guglielmo, M.; Fu
Prediction of myocardial blow flow under stress conditions by means of a computational model